

Collective vibrations of confined levitating droplets

S. J. Thomson,* M. M. P. Couchman, and J. W. M. Bush

Department of Mathematics, Massachusetts Institute of Technology, Cambridge, MA 02139

(Dated: December 21, 2024)

We report a new type of driven dissipative oscillator system consisting of a lattice of millimetric fluid droplets bouncing on a vertically vibrating liquid bath and bound within an annular ring. We characterize the system behaviour as it is energized through a progressive increase in the bath's vibrational acceleration. Depending on the number of drops, the onset of motion of the lattice may take the form of either out-of-phase oscillations or a striking solitary wave-like instability. Theoretical modelling demonstrates that this behaviour may be attributed to different bifurcations. Our results introduce a rich new direction for the study of non-equilibrium dynamical systems at the macroscale.

Wave propagation in active systems is an area of burgeoning interest and has been observed in a wide range of settings including bacterial suspensions [1–4]; fluids composed of synthetic micro-rollers and spinners [5–7]; and crystals of driven microfluidic water droplets [8–14]. Theoretical models of one-dimensional driven dissipative lattices exhibit instabilities in the form solitary waves, as well as unidirectional motion and out-of-phase (optical) oscillations [15–21]. However experimental realizations of such lattice systems are relatively scarce, limited to active electronic circuits [22–26]. We here present a robust new macroscopic realization of an active nonlinear lattice.

Millimetric droplets have been shown to bounce on the surface of a vibrating liquid bath or “walk” by means of self-propulsion through a resonant interaction with their own wave field [27–30]. In the bouncing state, the net wave force exerted on the drop by the bath supports its weight, enabling it to levitate above the bath surface, precluding coalescence. Above a critical vibrational acceleration, the droplet becomes unstable to small lateral perturbations. When the resulting propulsive wave force overcomes the stabilising effects of dissipation, the drop begins to walk [31]. Droplets brought into close proximity may interact and become coupled through their common wave field. While substantial progress has been made toward understanding the dynamics and stability of droplet pairs [32–38], the collective dynamics of many-droplet ensembles remains largely unexplored. We here consider the collective vibrations of an effectively one-dimensional lattice of coupled droplets (Figure 1(a)) as the vibrational acceleration of the bath is increased progressively. We demonstrate that this system exhibits canonical features of driven dissipative oscillator systems, including out-of-phase oscillations and solitary wave propagation. Using the model and stability analysis presented in [39], we rationalize the bifurcations responsible for these distinct dynamical states.

Our experimental set-up is based on that described in [40]. An annulus of inner radius $R_1 = 24$ mm and outer radius $R_2 = 31$ mm was placed in a stainless steel bath and mounted on an electromagnetic shaker. The bath

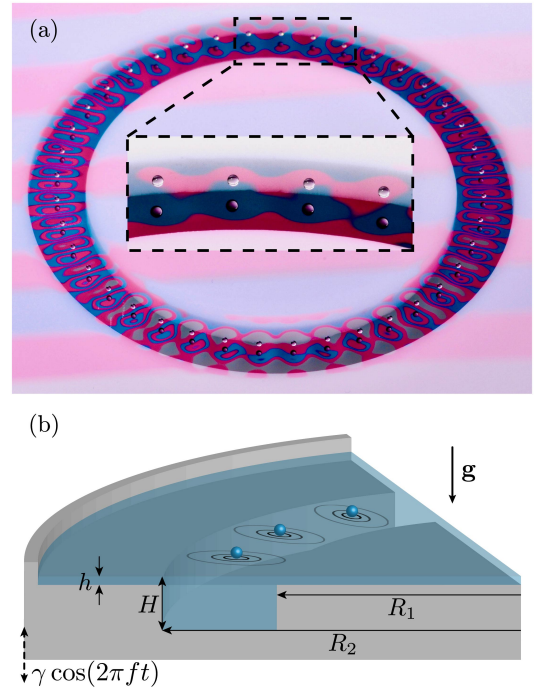


FIG. 1. (a) Oblique perspective of a chain of 40 equispaced droplets of silicone oil confined to an annular channel. (b) Schematic of the channel geometry with inner radius $R_1 = 24$ mm and outer radius $R_2 = 31$ mm. A shallow layer of depth $h = 0.56$ mm acts as a damper so that wave motion is largely confined to the channel where the fluid depth $H = 5.12$ mm. The entire assembly is vibrated vertically with maximum acceleration γ and frequency f .

was filled with silicone oil of density $\rho = 950$ kg m $^{-3}$, viscosity $\nu = 20$ cSt, and surface tension $\sigma = 20.6$ mN m $^{-1}$, to a depth $H = 5.12$ mm inside the annulus and $h = 0.56$ mm outside. The shallow region acts as a wave damper, ensuring that all droplet motion is confined to the channel [41, 42]. A schematic of our experiment is shown in Figure 1(b). The set-up was vibrated vertically with acceleration $a(t) = \gamma \cos(2\pi ft)$, where f and γ denote the frequency and maximum acceleration respectively. The vibration of the bath was monitored using two accelerometers and a closed-loop feedback en-

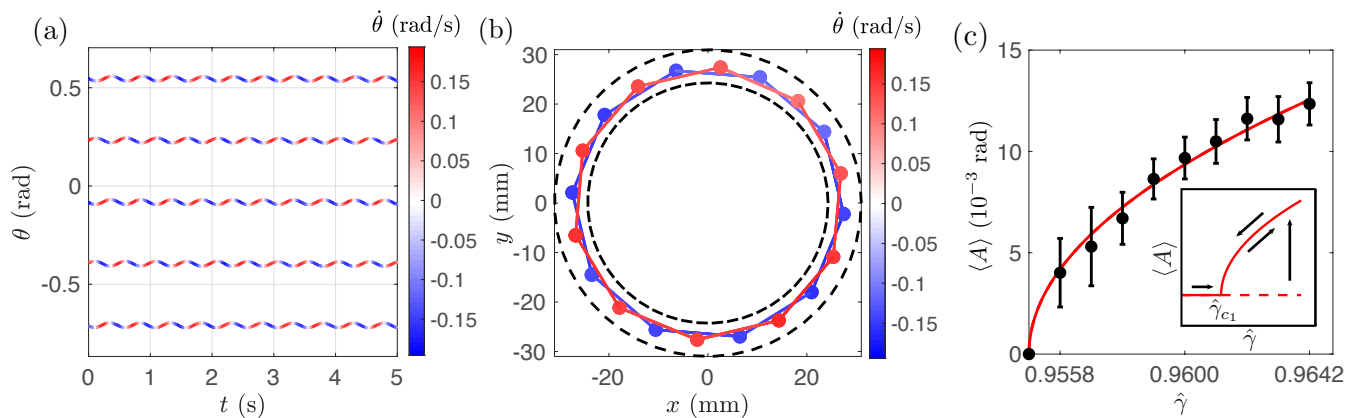


FIG. 2. $N = 20$ droplets. (a) Evolution of the polar angle θ of six adjacent droplets undergoing out-of-phase oscillations with frequency $F = 2$ Hz at vibrational acceleration $\hat{\gamma} = 0.962$. The trajectories are coloured according to the droplets' instantaneous angular velocity $\dot{\theta}$. Note that neighbouring droplets have equal and opposite $\dot{\theta}$ for all time t . (b) A snapshot of the polar positions of each droplet in the chain at a time when each droplet attains its maximum angular speed of $|\dot{\theta}| = 0.16$ rad s^{-1} . The value of $\hat{\gamma}$ is the same as in (a). The solid lines emphasise the net out-of-phase oscillation of two decahedral sub-lattices and the dashed lines delineate the channel geometry. (c) Plot of the mean oscillation amplitude $\langle A \rangle$ as a function of $\hat{\gamma}$ shows a monotonic increase of $\langle A \rangle$ beyond a critical value of $\hat{\gamma}_{c1} = 0.956$ and a saturation of the amplitude at higher $\hat{\gamma}$. The error bars represent the standard deviation of the mean. The red curve is a square-root-fit of the data. Inset: a schematic of the reversible supercritical bifurcation path underpinning the observed instability. The solid red line indicates the stable branch consisting of static then oscillating droplets; the dashed red line is unstable.

sured that γ was kept constant to within $\pm 0.002g$. The frequency f was fixed at 80 Hz. We note that a change in f can dramatically alter the system properties, influencing not only the wavelength of Faraday waves excited on the bath surface, and so the preferred interdroplet spacing, but the stability characteristics of the droplet lattice. For the chosen control parameters and geometry, the Faraday threshold (the critical vibrational acceleration above which waves form spontaneously on the bath surface) in the channel was found to be $\gamma_F = 4.72 \pm 0.05g$. Over time, the value of the Faraday threshold may slowly decrease due to the liquid temperature increasing and the concomitant decrease in viscosity [43]. In order to minimize this effect, the bath was vibrated for 1 hour at $\gamma > \gamma_F$ before the start of the experiment and γ_F was measured both before and after the experiment, its drift monitored.

Droplets of diameter $D = 0.72 \pm 0.01$ mm were generated using a piezoelectric drop generator and placed into the channel with the aid of a prewetted slide [44]. The presence of the channel largely restricts the droplet motion to one-dimension along the azimuthal direction θ , however the droplets are free to move slightly in the radial direction r . While the lattice was being formed, the bath was vibrated at $\gamma_B = 4g$. At γ_B , a single droplet bounces in resonance with its subcritical, subharmonic Faraday wave field, bouncing every two cycles of the bath [30, 45]. In what follows we describe the outcomes of two sets of experiments: one involving a chain of $N = 20$ droplets and the other $N = 40$ droplets.

In the two sets of experiments, all the droplets were

configured to have the same vertical bouncing phase and were arranged into a chain with a constant inter-droplet spacing, dictated by the superposition of wave fields generated by each individual droplet [46]. At equilibrium, the droplets sit at a radius of $R_m = 27.5$ mm and are separated by an angle $\Delta\theta = 2\pi/N$. The droplets are coupled by the wave fields excited by their neighbours, which effectively play the role of an inter-droplet potential. However we note that a novelty in our system is that this potential is not fixed in space with respect to the droplet; rather, it is generated by and evolves continuously with the droplet motion. To eliminate the influence of air currents, the bath was covered by a transparent acrylic box [47].

The acceleration of the bath was increased incrementally in steps of $0.01g$ from the initial value of γ_B until the stationary bouncing state destabilized. Thereafter, γ was varied in steps of $\Delta\gamma = 0.005g$ to increase the resolution of our data. The droplet positions were tracked using a CCD camera mounted directly above the bath, recording at 20 frames-per-second, and then processed using an in-house droplet-tracking algorithm in MATLAB. Henceforth, we characterize the proximity to the Faraday threshold in terms of the dimensionless vibrational acceleration $\hat{\gamma} = \gamma/\gamma_F$. At the beginning of the experiment, $\hat{\gamma}_B = 0.847$. For reference, the walking instability threshold of a single droplet $\hat{\gamma}_W = 0.873 \pm 0.02$.

With $N = 20$ droplets, the onset of instability was manifest as small azimuthal oscillations of the droplets about their equilibrium position. By increasing γ in small steps of $\Delta\gamma$, synchrony between the droplets emerged in

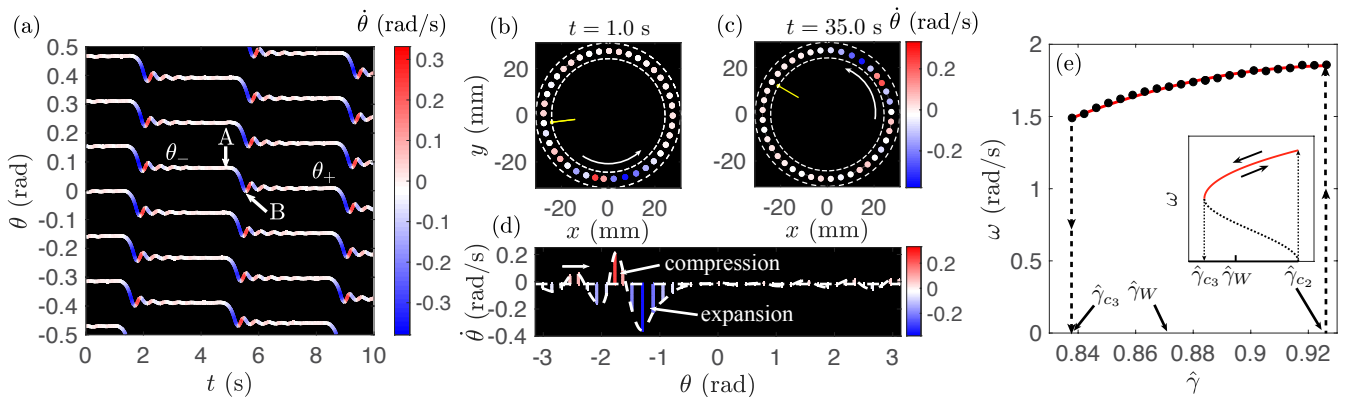


FIG. 3. $N = 40$ droplets. (a) Evolution of the angular position θ of individual droplets in the chain in the wave-propagation regime at vibrational acceleration $\hat{\gamma} = 0.890$. The trajectories are coloured according to the droplets' instantaneous angular velocity $\dot{\theta}$. Prior to the arrival of the wave at event A, a droplet is stationary at $\theta_- \approx 0.08$ rad. In the interval AB, it is pulled in the direction of decreasing θ over a time of order 0.5 s, reaching a maximum angular speed of $|\dot{\theta}| \sim 0.38$ rad s $^{-1}$. At event B, its angular speed returns to zero and thereafter the droplet settles down to $\theta_+ \approx 0$ rad *via* underdamped oscillations. (b)–(c) Polar positions of the droplets in the chain. Each droplet is coloured according to its instantaneous angular velocity. The value of $\hat{\gamma}$ is the same as that in (a). The yellow marker highlights the overall clockwise rotation of the lattice and white arrows show the direction of wave propagation. See [47] for a colour-coded animation of the polar droplet positions. (d) Droplet instantaneous angular velocity $\dot{\theta}$ as a function of droplet position at $t = 1$ s. We fit a cubic spline interpolant through the maximum of each spike, revealing a well-defined wave packet propagating in an anti-clockwise direction through the lattice. (e) Plot of $\omega(\hat{\gamma})$ (black dots). We find ω varies monotonically with $\hat{\gamma}$ but drops to zero at $\hat{\gamma}_{c3} = 0.839$. The best fit red curve emphasizes the nonlinearity of $\omega(\hat{\gamma})$. The maximum error in ω was found to be ± 0.01 rad s $^{-1}$. Inset: a schematic sketch of the subcritical bifurcation diagram underpinning the solitary wave instability. The upper solid red line (symbolic of the best fit line in the main plot) denotes the stable solitary wave branch, the dashed black curve a hypothetical unstable branch.

the form of out-of-phase oscillations (see [46] for an accompanying video). The motion of a subset of six droplet trajectories is plotted in Figure 2(a) for $\hat{\gamma} = 0.962$. Each droplet oscillates half a period out-of-phase with its neighbour with frequency $F = 2$ Hz. The net result of the instability is the out-of-phase oscillation of two decahedral sub-lattices (see Figure 2(b)). We determine the amplitude of oscillation as a function of $\hat{\gamma}$ by taking the mean oscillation amplitude $\langle A \rangle$ of all droplets in the chain. As shown in Figure 2(c), $\langle A \rangle$ increases monotonically from zero at $\hat{\gamma}_{c1} = 0.956 \pm 0.02$ and begins to plateau at higher $\hat{\gamma}$. We note that the error in $\hat{\gamma}_{c1}$ is due to a small hysteresis that arises when the instability threshold is approached from below or above [31, 48]. The foregoing observations point to a reversible supercritical bifurcation (see inset of Figure 2(c)) underpinning the observed instability.

With a lattice of $N = 40$ droplets, multiple realizations of the same experiment showed that the initial oscillatory state achieved with 20 drops cannot be sustained, with one droplet in the chain eventually receiving a large amplitude kick in the θ direction. A markedly different dynamics then ensued, namely the spontaneous excitation of a solitary wave that propagates around the ring indefinitely (see [46] for an accompanying video). The direction of propagation was either clockwise or counter-clockwise with equal probability. The dramatic transition to the solitary wave regime occurred

at $\hat{\gamma}_{c2} = 0.932 \pm 0.02$ and was observed in some instances to trigger a second wave following in the wake of the first. However it was found that this second wave could be suppressed by slightly reducing the acceleration. The experiments and accompanying data described here are for $\hat{\gamma} \in (0.839, 0.932)$, in which range a single solitary wave propagates around the lattice.

The wave progresses around the ring as each droplet successively undergoes the motion shown in Figure 3(a). Prior to the arrival of the wave an individual droplet is essentially stationary before being pulled sharply in the direction of decreasing θ . It then receives a restoring force in the opposite direction before settling down to a new equilibrium position *via* an underdamped oscillation. The initial jump in the droplet position gives rise to the curious feature that, while there is evidently a disturbance propagating in a counter-clockwise direction, the net displacement of the entire droplet lattice is clockwise, as indicated by the yellow marker in Figures 3(b) and (c). The wave field generated by each droplet has a spatial extent exceeding the equilibrium droplet spacing; hence, each droplet influences more than its nearest neighbour. This is evident in Figures 3(b)–(d), which show that the current position of the wave is marked by a core of approximately 7 droplets undergoing different stages of the motion described in Figure 3(a). Following the passage of the wave, the droplets oscillate back and forth and eventually recover their uniform initial spacing.

After increasing the acceleration so as to excite a solitary wave, we computed ω , the angular frequency of the wave, as a function of $\hat{\gamma}$ in the interval $\hat{\gamma} \in (0.839, 0.932)$, which revealed a monotonic relationship between the two (see Figure 3(e)). We note that, in contrast to the $N = 20$ case, this interval contains the walking threshold of a single droplet $\hat{\gamma}_W = 0.873$. Determining $\omega(\hat{\gamma})$ revealed two further differences with the case of $N = 20$ droplets. First, we find that the solitary wave can propagate without decay far below the initial instability threshold of the stationary lattice $\hat{\gamma}_{c_2}$, specifically for $\hat{\gamma} < \hat{\gamma}_W$. Second, we find that there is a critical value $\hat{\gamma}_{c_3} = 0.839$ at which ω jumps *discontinuously* to zero from a finite value (for a video of this transition see [46]). We thus deduce the co-existence of two qualitatively different stable states of the system for $\hat{\gamma} \in (0.839, 0.932)$: the static equilibrium configuration of the bouncing droplets and a periodic state consisting of the solitary wave. The foregoing observations suggest that the system has undergone a subcritical bifurcation. A sketch of the associated hysteresis path is plotted in the inset of Figure 3(e) and is to be contrasted with that of Figure 2(c). In the parlance of dynamical systems, the point $\hat{\gamma}_{c_3}$ is reminiscent of a saddle node or blue-sky bifurcation [49].

We now summarize the modelling and stability analysis presented in [39], aimed at rationalizing qualitatively the different bifurcation structures that can arise as the number of droplets N varies. To model our system close to the point of instability, [39] considers the scenario in which N equispaced droplets lie on a circle of constant radius R . The arc-length position of each drop x_n evolves according to the stroboscopic model derived by Oza *et al.* [50]. In dimensionless form, the droplet motion is described by a balance between inertia, drag, and the propulsive wave force, namely

$$\ddot{x}_n + \dot{x}_n = -\mathcal{H}_x(x_n, t), \quad (1)$$

where the wave field

$$\mathcal{H} = \sum_{m=1}^N \int_{-\infty}^t \mathcal{K}(x - x_m(s)) e^{-(t-s)/M} ds \quad (2)$$

is written as a superposition of the wave fields generated by each droplet in the lattice. Following [39], the kernel $\mathcal{K}(x) = f(2R \sin(x/2R))$ is taken as a circular cut of radius R of the axisymmetric wave field $f(r) = \mathcal{A} J_0(2\pi r) \operatorname{sech}(r/l)$, centered a distance R from the origin. The parameter l is the dimensionless decay length of the waves relative to the Faraday wavelength, \mathcal{A} is the wave amplitude, and $M \propto (1 - \hat{\gamma})^{-1}$ encodes the exponential decay time of the waves.

The stability characteristics of the lattice may be rationalized qualitatively by a weakly-nonlinear analysis of the system (1)–(2). The key feature of this analysis is that, close to the bifurcation point $M = M_c$ (that

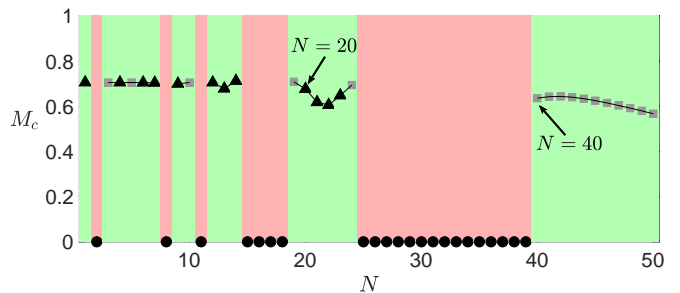


FIG. 4. Plot of the stability threshold M_c versus droplet number N . Triangles mark supercritical bifurcations ($\Re(\beta_2) > 0$) and squares mark subcritical bifurcations ($\Re(\beta_2) < 0$) as predicted by Equation (3). Red zones and circles mark droplet configurations that our theory predicts are unstable for all M in this one-dimensional setting. The parameter values used are $R = 5.4$, $l = 1.6$, and $\mathcal{A} = 0.1$. Figure adapted, with permission, from [39].

is, $M - M_c = \varepsilon^2$, where $\varepsilon \ll 1$), the complex amplitude A of the perturbation to the n -th droplet position, $\hat{x}_n = A(T) \exp(i(k_c n \alpha + \omega_c t)) + \text{c.c.}$, may be described by a Stuart-Landau equation of the form

$$\frac{dA}{dT} = \beta_1(N)A - \beta_2(N)|A|^2 A, \quad (3)$$

where the droplet separation $\alpha = 2\pi/N$ and A is a function of the slow time-scale $T = \varepsilon^2 t$. The critical wavenumber k_c and angular frequency ω_c are determined from the linear stability of (1)–(2). The crucial component of (3) is the sign of $\Re(\beta_2)$, defined in terms of the system parameters. For $\Re(\beta_2) > 0$ the cubic nonlinearity stabilizes linear growth, leading to a supercritical bifurcation, while $\Re(\beta_2) < 0$ heralds a subcritical bifurcation.

In Figure 4 we plot the critical value of M_c at which each lattice configuration destabilises given N , as deduced from the computations in [39]. We note that, in all cases contained within green zones of Figure 4, the system was found to undergo a Hopf bifurcation [49]. Red zones are cases in this one-dimensional setting where the wavefield h acts to destabilise the droplets for all M , as can occur if a droplet sits on a peak of the lattice wave field [38]. The precise details of this figure depend on the parameter values and choice of wave kernel \mathcal{K} ; nevertheless we see that it captures the critical features of our experimental observations. In the supercritical case $N = 20$, where linear theory predicts $k_c = N/2$, we find $\hat{x}_n \propto (-1)^n \cos(\Omega t)$ corresponding to out-of-phase oscillations (recall Figure 2(c)), the angular frequency Ω being determined as part of the weakly-nonlinear analysis. For $N \geq 40$ and tightly packed droplets, there is a prevalence of subcritical bifurcations wherein the system approaches a distant attractor, manifest in experiments as a solitary wave (Figure 3(e)).

We have considered the collective vibrations of a new type of driven dissipative oscillator, which exhibits out-

of-phase oscillations and solitary waves. The former is characterised by the onset of a reversible supercritical bifurcation where the amplitude of the oscillations increases with the driving acceleration. The latter subcritical bifurcation displays the coexistence of two distinct stable states, one static, the other characterized by a solitary wave whose angular frequency ω has a non-linear dependence on $\hat{\gamma}$. The transition between these two regimes has been rationalised through a systematic stability analysis in the vicinity of the bifurcation point [39]. A detailed description of the fully nonlinear dynamics of the system, including modelling of the fluid [51], is subject to future work. The results presented here raise several interesting questions regarding solitary waves in mechanical systems [52–54] and emergent phenomena in active media, rendered accessible through our highly-tunable experimental set-up.

S.J.T would like to thank Matthew Durey and Rodolfo R. Rosales, with whom valuable discussions were had regarding the different bifurcations outlined in this paper, prompting the careful data acquisition leading to Figures 2(c) and 3(e). The authors would also like to thank two anonymous referees whose suggestions led to the improvement of this manuscript.

The datasets used in this study are available from the corresponding author upon reasonable request.

* Corresponding author: thomsons@mit.edu

- [1] A. Lefaue and D. Saintillan, *Physical Review E* **89**, 021002 (2014).
- [2] A. Creppy, F. Plouraboué, O. Praud, X. Druart, S. Cazin, H. Yu, and P. Degond, *Journal of The Royal Society Interface* **13**, 20160575 (2016).
- [3] H. Wioland, E. Lushi, and R. E. Goldstein, *New Journal of Physics* **18**, 075002 (2016).
- [4] M. Theillard, R. Alonso-Matilla, and D. Saintillan, *Soft Matter* **13**, 363 (2017).
- [5] A. Bricard, J.-B. Caussin, D. Das, C. Savoie, V. Chikkadi, K. Shitara, O. Chepizhko, F. Peruani, D. Saintillan, and D. Bartolo, *Nature Communications* **6**, 7470 (2015).
- [6] D. Geyer, A. Morin, and D. Bartolo, *Nature Materials* **17**, 789 (2018).
- [7] V. Soni, E. S. Bililign, S. Magkiriadou, S. Sacanna, D. Bartolo, M. J. Shelley, and W. T. Irvine, *Nature Physics*, 1 (2019).
- [8] T. Beatus, T. Tlusty, and R. Bar-Ziv, *Nature Physics* **2**, 743 (2006).
- [9] T. Beatus, R. Bar-Ziv, and T. Tlusty, *Physical Review Letters* **99**, 124502 (2007).
- [10] M. Baron, J. Bławdziewicz, and E. Wajnryb, *Physical Review Letters* **100**, 174502 (2008).
- [11] T. Beatus, R. H. Bar-Ziv, and T. Tlusty, *Physics Reports* **516**, 103 (2012).
- [12] P. Janssen, M. Baron, P. Anderson, J. Bławdziewicz, M. Loewenberg, and E. Wajnryb, *Soft Matter* **8**, 7495 (2012).
- [13] U. D. Schiller, J.-B. Fleury, R. Seemann, and G. Gompper, *Soft Matter* **11**, 5850 (2015).
- [14] A. C. H. Tsang, M. J. Shelley, and E. Kanso, *Soft Matter* **14**, 945 (2018).
- [15] W. Ebeling, U. Erdmann, J. Dunkel, and M. Janssen, *Journal of Statistical Physics* **101**, 443 (2000).
- [16] V. A. Makarov, W. Ebeling, and M. G. Velarde, *International Journal of Bifurcation and Chaos* **10**, 1075 (2000).
- [17] J. Dunkel, W. Ebeling, U. Erdmann, and V. A. Makarov, *International Journal of Bifurcation and Chaos* **12**, 2359 (2002).
- [18] A. Chetverikov and J. Dunkel, *The European Physical Journal B: Condensed Matter and Complex Systems* **35**, 239 (2003).
- [19] A. P. Chetverikov, W. Ebeling, and M. G. Velarde, *International Journal of Bifurcation and Chaos* **16**, 1613 (2006).
- [20] A. P. Chetverikov, K. S. Sergeev, and E. del Rio, *International Journal of Bifurcation and Chaos* **28**, 1830027 (2018).
- [21] A. Chetverikov, K. Sergeev, and E. del Rio, *Physica A: Statistical Mechanics and its Applications* **513**, 147 (2019).
- [22] R. Hirota and K. Suzuki, *Proceedings of the IEEE* **61**, 1483 (1973).
- [23] A. C. Singer and A. V. Oppenheim, *International Journal of Bifurcation and Chaos* **9**, 571 (1999).
- [24] V. Makarov, E. Del Rio, W. Ebeling, and M. Velarde, *Physical Review E* **64**, 036601 (2001).
- [25] V. I. Nekorkin and M. G. Velarde, *Synergetic phenomena in active lattices: patterns, waves, solitons, chaos* (Springer Science & Business Media, 2012).
- [26] T. Kotwal, H. Ronellenfitsch, F. Moseley, and J. Dunkel, *arXiv preprint* (2019), arXiv:1903.10130.
- [27] Y. Couder, E. Fort, C.-H. Gautier, and A. Boudaoud, *Physical Review Letters* **94**, 177801 (2005).
- [28] Y. Couder, S. Protière, E. Fort, and A. Boudaoud, *Nature* **437**, 208 (2005).
- [29] S. Protière, A. Boudaoud, and Y. Couder, *Journal of Fluid Mechanics* **554**, 85 (2006).
- [30] J. W. M. Bush, *Annual Review of Fluid Mechanics* **47**, 269 (2015).
- [31] J. Moláček and J. W. M. Bush, *Journal of Fluid Mechanics* **727**, 582 (2013).
- [32] S. Protière, S. Bohn, and Y. Couder, *Physical Review E* **78**, 036204 (2008).
- [33] A. Eddi, J. Moukhtar, S. Perrard, E. Fort, and Y. Couder, *Physical Review Letters* **108**, 264503 (2012).
- [34] C. Borghesi, J. Moukhtar, M. Labousse, A. Eddi, E. Fort, and Y. Couder, *Physical Review E* **90**, 063017 (2014).
- [35] A. U. Oza, E. Siéfert, D. M. Harris, J. Moláček, and J. W. M. Bush, *Physical Review Fluids* **2**, 053601 (2017).
- [36] J. Arbeláiz, A. U. Oza, and J. W. M. Bush, *Physical Review Fluids* **3**, 013604 (2018).
- [37] C. Galeano-Rios, M. M. P. Couchman, P. Caldairou, and J. W. M. Bush, *Chaos: An Interdisciplinary Journal of Nonlinear Science* **28**, 096112 (2018).
- [38] M. M. P. Couchman, S. E. Turton, and J. W. M. Bush, *Journal of Fluid Mechanics* **871**, 212 (2019).
- [39] S. J. Thomson, M. Durey, and R. R. Rosales, (2020), (in preparation).
- [40] D. M. Harris and J. W. M. Bush, *Journal of Sound and Vibration* **334**, 255 (2015).
- [41] B. Filoux, M. Hubert, and N. Vandewalle, *Physical Re-*

- view E **92**, 041004 (2015).
- [42] B. Filoux, M. Hubert, P. Schlagheck, and N. Vandewalle, *Physical Review Fluids* **2**, 013601 (2017).
- [43] D. M. Harris and J. W. M. Bush, *Journal of Fluid Mechanics* **739**, 444 (2014).
- [44] D. M. Harris, T. Liu, and J. W. M. Bush, *Experiments in Fluids* **56**, 83 (2015).
- [45] J. Moláček and J. W. M. Bush, *Journal of Fluid Mechanics* **727**, 612 (2013).
- [46] See Supplemental Material at xxx for access to all experimental videos and supporting materials referenced in this paper.
- [47] G. Pucci, D. M. Harris, L. M. Faria, and J. W. M. Bush, *Journal of Fluid Mechanics* **835**, 1136 (2018).
- [48] Ø. Wind-Willassen, J. Moláček, D. M. Harris, and J. W. M. Bush, *Physics of Fluids* **25**, 082002 (2013).
- [49] S. H. Strogatz, *Nonlinear Dynamics and Chaos: With Applications to Physics, Biology, Chemistry, and Engineering* (CRC Press, 2018).
- [50] A. U. Oza, R. R. Rosales, and J. W. M. Bush, *Journal of Fluid Mechanics* **737**, 552 (2013).
- [51] M. Durey, P. A. Milewski, and Z. Wang, *Journal of Fluid Mechanics* (2020), (under review).
- [52] C. Coste, E. Falcon, and S. Fauve, *Physical Review E* **56**, 6104 (1997).
- [53] B. Deng, J. R. Raney, V. Tournat, and K. Bertoldi, *Physical Review Letters* **118**, 204102 (2017).
- [54] Y. Zhang, B. Li, Q. S. Zheng, G. M. Genin, and C. Q. Chen, *Nature Communications* **10**, 1 (2019).